PHYSICAL REVIEW B **96**, 100202(R) (2017)

Photonic Chern insulator through homogenization of an array of particles

Meng Xiao and Shanhui Fan*

Department of Electrical Engineering and Ginzton Laboratory, Stanford University, Stanford, California 94305, USA

(Received 21 April 2017; published 28 September 2017)

We propose a route towards creating a metamaterial that behaves as a photonic Chern insulator, through homogenization of an array of gyromagnetic cylinders. We show that such an array can exhibit nontrivial topological effects, including topologically nontrivial band gaps and one-way edge states, when it can be homogenized to an effective medium model that has the Berry curvature strongly peaked at the wave vector $k = 0$. The nontrivial band topology depends only on the parameters of the cylinders and the cylinders' density, and can be realized in a wide variety of different lattices, including periodic, quasiperiodic, and random lattices. Our system provides a platform to explore the interplay between disorder and topology and also opens a route towards the synthesis of topological metamaterials based on the self-assembly approach.

DOI: 10.1103/PhysRevB.96.100202

The classification of band structures in terms of band topology in classical waves has led to the newly emerging field of topological photonics and phononics [1–32]. The majority of previous works on topological photonics and phononics consider periodic structures, where nontrivial topology arises from the scattering of waves by the periodic structure. Complementary to the developments of topological photonic and phononic crystals, however, there have also been significant recent works on topological metamaterials [29–33]. In these designs of topological metamaterials, one considered a uniform system as characterized by an electromagnetic susceptibility such as a permittivity or permeability tensor, and identified nontrivial topological features in the band structure associated with such a susceptibility.

Since the possible susceptibilities of naturally occurring materials are rather limited, for the vast majority of works on metamaterials, one considers an inhomogeneous system consisting of an array of meta-atoms, and obtains its effective susceptibility, which defines the corresponding effective medium through a homogenization procedure. Therefore, a question that is central to the development of topological metamaterial naturally arises: To what extent does the homogenization procedure preserve topological properties? This is to say, for a given effective medium that has topological features, can one construct a physical system consisting of an array of meta-atoms, which homogenizes to such an effective medium, and exhibits some of the nontrivial topological properties? This question, which is of central importance to the physical implementation of topological metamaterials, has not been addressed in previous literature on topological metamaterials and in fact is quite subtle. In spite of the existence of standard homogenization procedures, it is far from obvious, *a priori*, that the topology of a physical metamaterial system consisting of an array of subwavelength elements can be understood in terms of its effective medium, regardless of whether such an effective medium is local or nonlocal. For an effective medium model to work, the effective wavelength, which is the length scale at which the field varies, should be much larger than the size of the unit cell. Since at the Brillouin zone boundary, the effective wavelength is always comparable with the size of the unit cell, there is no guarantee that an effective medium model can be used to obtain the information about the band structure over the entire first Brillouin zone. Yet such information is necessary to determine the topology (such as the Chern number) of the band structure.

In this Rapid Communication, we address the question above by constructing an effective medium in which the Berry curvature of its band structure is strongly peaked at $k = 0$, where k is the wave vector. Since the effective medium model should describe the physical structure very well near $k = 0$, we expect that the nontrivial band topology of the effective medium model should also manifest in physical metamaterial systems. Indeed, through numerical simulations, we find that our metamaterial systems with a wide variety of lattices, including periodic, quasiperiodic, and random lattices, all of which homogenize to the same effective medium model, all possess complete nontrivial topological band gaps. We also note that only parts of the topological features of the effective medium persist in the inhomogeneous physical system.

From a fundamental physics perspective, the systems that we consider here may provide a platform to explore the interplay between order or disorder and topology. From an experimental perspective, creating a disordered system with nontrivial topology may relax the stringent requirements for fabricating topologically nontrivial photonic and phononic systems. While there have been several very recent works on nontrivial topological photonic structures utilizing aperiodic lattices [34–36], our construction differs in that it is not based on any specific lattice [34,35] or needs to engineer the local connections [36]. The structure reported here may therefore open a route towards the synthesis of topological metamaterials based on the self-assembly approach [37–39].

We first introduce an effective medium model that exhibits nontrivial topology in its band structure, and has the Berry curvature of its band structure strongly peaked at $k = 0$. We consider electromagnetic waves in two dimensions and focus on the transverse magnetic (TM) polarization, which has the electric field E_z along the z direction and the magnetic field H_x, H_y in the xy plane. For such a TM polarized wave, we consider an effective medium model where the relevant effective electromagnetic materials are the relative electric permittivity ε_e along the z direction, and the relative magnetic permeability in the xy plane, which has the form

*Corresponding author: shanhui@stanford.edu

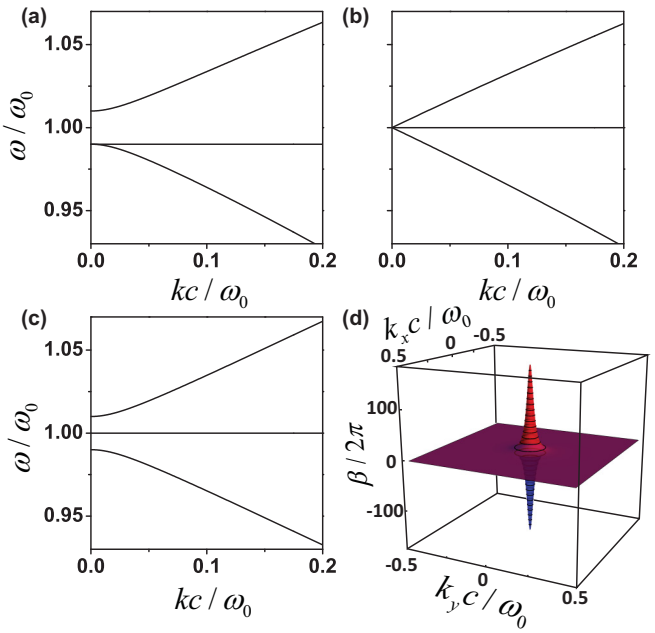

FIG. 1. The dispersion relation for the system as described by Eq. (1) with $\gamma_\varepsilon = \gamma_\mu = 3$. ω_0 is a reference frequency, c is the speed of light in vacuum, and k is the in-plane wave vector. (a) $\omega_E = 1.01\omega_0$, $\omega_H = 0.99\omega_0$, $\mu_k = 0$. (b) $\omega_E = \omega_H = \omega_0$ and $\mu_k = 0$. (c) $\omega_E = \omega_H = \omega_0$ and $\mu_k = 0.03$. (d) Red and blue represent the Berry flux β of the highest and lowest bands in (c), respectively. The Berry flux of the middle band in (c) is exactly zero.

$\ddot{\mu}_e = (\mu_r, i\mu_k; -i\mu_k, \mu_r)$. In order to achieve a band structure with nontrivial topology, we start with the case where $\mu_k = 0$, and

$$\varepsilon_e = \gamma_\varepsilon(\omega - \omega_E)/\omega_E,$$
$$\mu_r = \gamma_\mu(\omega - \omega_H)/\omega_H. \tag{1}$$

The starting point for our system is therefore the epsilon and mu near zero (EMNZ) systems that have been widely considered in the metamaterial literature [40]. Here, we consider a lossless system. γ_e and γ_μ are both positive, as required by causality [41]. When $\omega_E \neq \omega_H$ [Fig. 1(a)], the system supports a mode that is singly degenerate at $k = 0$ having a frequency $\omega = \omega_E$. This mode exhibits a quadratic dispersion at $k \neq 0$. The system also supports at $k = 0$ a pair of doubly degenerate modes at $\omega = \omega_H$. At $k \neq 0$ the two modes split into two bands, one with flat dispersion and the other with quadratic dispersion. By setting $\omega_E = \omega_H \equiv \omega_0$, we force a threefold accidental degeneracy at $k = 0$ [42,43]. At $k \neq 0$, the three modes split into two bands with a Dirac-like linear dispersion as well as a flatband, as shown in Fig. 1(b).

Starting with the band structure in Fig. 1(b), we then break time-reversal symmetry by setting a frequency-independent $\mu_k \neq 0$. Now the threefold degeneracy at $k = 0$ is completely lifted, as shown in Fig. 1(c), and two band gaps are introduced into the system. Both of these band gaps are topologically nontrivial. To see the nontrivial topology, here we develop a Hamiltonian for the Maxwell's equations near ω_0. For the system with $\mu_k = 0$, an effective Hamiltonian has been developed to describe the physics in the vicinity of the triply degenerate point [44]. For our system here with $\mu_k \neq 0$, starting from the Maxwell's equations, and keeping only the lowest order of $\Delta\omega \equiv \omega - \omega_0$, we obtain

$$\begin{pmatrix} 0 & -i\tilde{\mu}_k & \tilde{k}_y \\ i\tilde{\mu}_k & 0 & -\tilde{k}_x \\ \tilde{k}_y & -\tilde{k}_x & 0 \end{pmatrix} \begin{pmatrix} \tilde{H}_x \\ \tilde{H}_y \\ \tilde{E}_z \end{pmatrix} = \frac{\Delta\omega}{\omega_E} \begin{pmatrix} \tilde{H}_x \\ \tilde{H}_y \\ \tilde{E}_z \end{pmatrix}, \tag{2}$$

where $\tilde{\mu}_k = \mu_k/\gamma_\mu$, $\tilde{k}_{x,y} = k_{x,y}c/(\omega_0\sqrt{\gamma_\varepsilon\gamma_\mu})$, $\tilde{H}_{x,y} = \sqrt{\mu_0\gamma_\mu}H_{x,y}$, $\tilde{E}_z = \sqrt{\varepsilon_0\gamma_\varepsilon}E_z$, and c is the speed of light. Here, k_x and k_y are the wave vectors, respectively. The matrix on the right-hand side of Eq. (2) can now serve as an effective Hamiltonian. The three eigenvalues of this Hamiltonian are given by $\{0, \pm\sqrt{\tilde{k}_x^2 + \tilde{k}_y^2 + \tilde{\mu}_k^2}\}$, which is consistent with the band dispersion in Fig. 1(c). With the effective Hamiltonian obtained, we can determine the total Berry flux for the upper, middle, and lower bands to be $-\mathrm{sgn}(\mu_k)2\pi$, 0, and $\mathrm{sgn}(\mu_k)2\pi$, respectively, when $\mu_k \neq 0$. Thus we have introduced an effective medium model with topologically nontrivial band gaps. Such an effective medium model thus represents a photonic Chern insulator. While there have been many theoretical proposals and experimental demonstrations of photonic Chern insulators [4–9], the effective medium model as proposed here represents another route for creating a Chern insulator. In this model, the Berry curvature peaks at $k = 0$, as shown in Fig. 1(d). Therefore, we anticipate that this effective medium model can be used to guide the construction of physical metamaterial structures through homogenization.

Motivated by the effective medium model as presented above, we now consider physical metamaterial systems which homogenize to this model at $k = 0$. We first consider an individual cylinder with radius r_c, relative permittivity ε_c, and the relative permeability in the xy plane $\ddot{\mu}_c = (1, i\kappa; -i\kappa, 1)$, where κ is assumed to be frequency independent. This is a simplified model for gyromagnetic effects. A more sophisticated model of the gyromagnetic effects can be found in Ref. [44]. The main results of this Rapid Communication are not affected by the use of the more sophisticated model. The electric and magnetic dipole responses of a cylinder are described by $\vec{p} = \varepsilon_0\alpha_E\vec{E}^{\mathrm{loc}}$ and $\vec{m}_\pm = \alpha_\pm\vec{H}^{\mathrm{loc}}$, where $\vec{E}^{\mathrm{loc}}$ and $\vec{H}^{\mathrm{loc}}$ represent the local electric and magnetic fields, respectively, α_E and $\alpha_\pm$ represent respectively the electric and magnetic dipole polarizabilities, and can be found in Supplemental Material Sec. I [45].

We then consider a metamaterial system consisting of an array of cylinders as described above. An example of such a metamaterial is shown in Fig. 2(a). Following the procedure in Ref. [46], we derive the effective medium parameters by solving the scattering problem as illustrated in Fig. 2(b). Here, one particle is set at the center of a cylindrical cavity filled with air and surrounded by a background consisting of the effective medium. The radius of the cylindrical cavity r_0 is chosen such that $\pi r_0^2/a^2 = 1$, where $1/a^2$ is the number of cylinders inside a unit area for the random array. The parameters of the effective medium are determined by assuming that there is no scattering by the cavity for waves incident from the effective medium in the limit where the wavelength in the effective medium is much larger than r_0, in which case only the electric and magnetic dipole responses of the cylinder

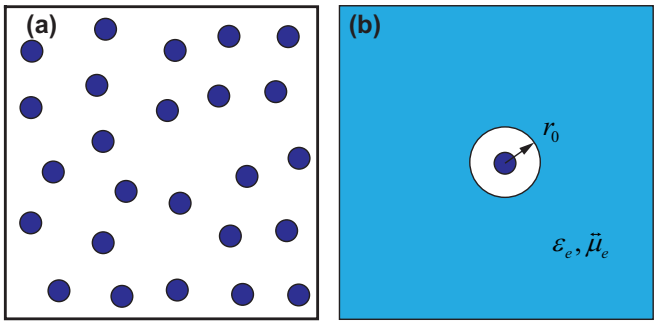

FIG. 2. (a) A system consisting of a random array of cylindrical particles (solid blue disks). Each particle is described by its electric and magnetic dipole responses to external electromagnetic fields. There are in total 25 cylinders with the same radius in (a). The cylinders are randomly distributed with equal probability while keeping the minimal distances between cylinders to be larger than $0.8a$, where $1/a^2$ represents the density of the cylinder. (b) A sketch showing the geometry used in deriving the effective parameters ε_e and $\vec{\mu}_e$, which provide an effective medium model for the array in (a). The light blue regions are filled uniformly with material having such effective parameters.

need to be taken into account. The no-scattering condition gives (refer to Supplemental Material Sec. I [45] for detailed derivations)

$$\varepsilon_e = -\frac{2\left[4J'_0(k_0r_0) + i\alpha_E k_0^2 H_0^{(1)'}(k_0r_0)\right]}{k_0r_0\left[4J_0(k_0r_0) + i\alpha_E k_0^2 H_0^{(1)}(k_0r_0)\right]}, \tag{3}$$

and

$$\mu'_r \mp \mu'_k = \frac{k_0r_0\left[8J'_1(k_0r_0) + i\alpha_\pm k_0^2 H_1^{(1)'}(k_0r_0)\right]}{\left[8J_1(k_0r_0) + i\alpha_\pm k_0^2 H_1^{(1)}(k_0r_0)\right]}, \tag{4}$$

with $\mu_k = -\mu'_k/(\mu'^2_r - \mu'^2_k)$, $\mu_r = \mu'_r/(\mu'^2_r - \mu'^2_k)$, and k_0 is the wave vector in vacuum. $J_n(x)$, $H_n^{(1)}(x)$, $J'_n(x)$, and $H_n^{(1)\prime}(x)$ are the Bessel functions and Hankel functions of the first kind and their derivatives. It can be proved that the effective parameters as described in Eqs. (3) and (4) are purely real when the system is nonabsorptive [46] (see also Supplemental Material Sec. I [45]). When the time-reversal symmetry is preserved, i.e., when $\kappa = 0$ in $\vec{\mu}_c$, the effective parameters having the form of Eq. (1) can be achieved by choosing the parameters of the cylinders such that the electric and magnet dipole responses have the same resonant frequencies, which then results in the dispersion relation shown in Fig. 1(b) [42]. Starting from such a cylinder, the dispersion relation in Fig. 1(c) can then be achieved by setting $\kappa \neq 0$ in $\vec{\mu}_c$, which breaks the time-reversal symmetry.

Using full wave simulations, we now show that different lattices of the cylinders as discussed above, all of which homogenize to the same effective medium model as described above, in fact, all possess nontrivial topology in their band structures. In Fig. 3(a), we consider the square lattice case. The cylinders have the parameters $r_c = 0.1735a$, $\varepsilon_c = 20$, and $\kappa = 0$, which are determined following the homogenization procedure as outlined above. The threefold degeneracy at the

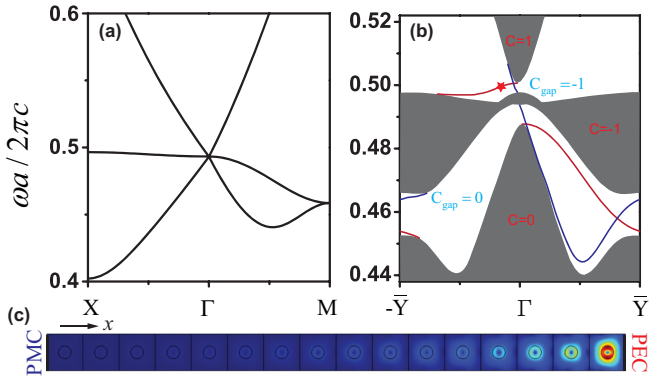

FIG. 3. (a) The band structure of cylinders in a square lattice. (b) Projected band structure (gray area) and corresponding surface states with the supercell in (c). This supercell is terminated by a PMC boundary on the left and a PEC boundary on the right. Here, red and blue curves represent the surface states at the PEC and PMC boundaries, respectively. The Chern numbers for the band and the gap Chern numbers in (b) are labeled in red and cyan, respectively. The electric field amplitude of the surface state marked by a red star ($k_y a/\pi = -0.2$) in (b) is also shown in (c), where red and blue colors represent maximum and zero field amplitudes, respectively. The cylinder has a radius of $r_c = 0.1735a$, where a represents the lattice constant of the square lattice. The relative permittivity of the cylinders is $\epsilon_c = 20$. $\kappa = 0$ in (a) and $\kappa = 0.08$ in (b) and (c).

Γ point (i.e., $k = 0$ point) and conical-like dispersion near the Γ point are consistent with the effective model as plotted in Fig. 1(b). In fact, we can find similar band dispersions near the Γ point as those in Figs. 1(a)–1(c) by varying some of the parameters of the cylinders (see Supplemental Material Sec. II [45]). Based on the square lattice discussed above, we now consider the strip geometry shown in Fig. 3(c). The lattice consists of the same cylinder as discussed above but with $\kappa = 0.08$. The lattice is periodic along the y direction and truncated by a perfect magnetic conductor (PMC) boundary on the left and a perfect electric conductor (PEC) boundary on the right. The projected band and the corresponding surface states are shown in Fig. 3(b). The field distribution of one of the surface states near the PEC boundary is also shown in Fig. 3(c). The projected band structure consists of three groups of bulk bands. Dispersions of the upper and lower groups of bulk bands agree well with the effective medium model near the Γ point. And as predicted by the effective medium model, the breaking of time-reversal symmetry introduces a local Berry flux of 2π and one-way surface states emerge near the Γ point.

On the other hand, the effective medium model does not describe the band structure for the wave vectors significantly away from the Γ point. First, the middle band is no longer perfectly flat. Second, as shown in Fig. 3(a), there exists a band degeneracy between the lower two bands at the M point protected by a combination of time-reversal symmetry and the C_{4v} lattice symmetry. Such degeneracy is not predicted by our effective medium model. When this degeneracy is lifted by breaking the time-reversal symmetry, a Berry flux of 2π peaks at the M point, and as a result, the lower band becomes topologically trivial. The surface states inside the lower band gap emerge near the Γ point, almost reach the other band, but then merge back into their original bands.

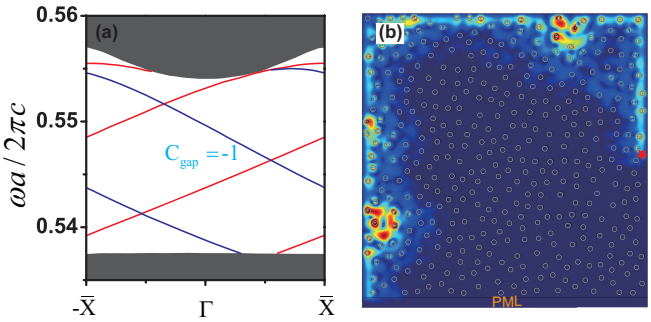

FIG. 4. (a) The projected bulk band structure (gray regions) and the band structure of surface states (red and blue curves) of a strip geometry consists of five of the supercells, each of which is shown in Fig. 2(a). The upper and lower boundaries of the strip are terminated by PECs and the strip is periodic along the horizontal direction. The blue and red curves represent the surface states on the upper boundary and the lower boundary, respectively. (b) One-way edge modes supported by a finite random lattice of cylinders. Here, the red star marks the position of the source with an operating frequency at $\omega a/(2\pi c) = 0.547$. The rectangles on the lower end of the figure represent a perfectly matched layer (PML) region that absorbs the waves. All the other outer boundaries in (b) are PEC. The radius of the cylinder and the relative permittivity are $r_c = 0.1735a$ and 20, respectively, where $1/a^2$ is the density of the cylinders, and $\kappa = 0.4$.

In the square lattice structure, we observe that the effective medium model of Fig. 3 generally agrees well with the band structure of the physical system near the Γ point. Moreover, the upper band of Fig. 3 in the effective medium model agrees quite well with the band structure of the physical system. As a result, one can achieve a topologically nontrivial band gap between the upper and the middle bands in the physical systems. A one-way edge state can be found in such a band gap in a truncated lattice. The lower band, on the other, significantly differs from the effective medium model away from Γ. These observations turn out to be generally applicable for other lattices that homogenize to the same effective medium model. As an additional example, results for a triangular lattice are shown in Supplemental Material Sec. III [45]. Therefore, we have shown that the effective medium model as we have developed here provides the guidance for creating a class of nontrivial topological metamaterials with different periodic lattices.

We now show that the effective medium model can be used to guide us in constructing random or quasiperiodic systems with a nontrivial topological band gap and a one-way edge state. The evolution of the band structures from a square lattice to a completely random lattice is discussed in Supplemental Material Sec. VI [45]. As an exemplary demonstration of random systems, we consider a geometry with a supercell as shown in Fig. 2(a). The supercell forms a square lattice and each supercell contains 25 cylinders with the same radius, dielectric constant, and density of cylinders as in Fig. 3(b), except with $\kappa = 0.4$. Within each supercell, the cylinders are randomly distributed with equal probability while keeping the minimal distances between cylinders to be larger than $0.8a$ so that the dipole approximation remains valid. The projected band structure for a strip geometry with five supercells along the y direction is shown in Fig. 4(a). The strip is truncated in the y direction with PEC boundaries on the upper and lower sides, and is assumed to be periodic along the x direction. The structure supports a topological nontrivial band gap, the frequency range of which corresponds to the upper band gap in the effective medium model. Within the gap the structure supports one-way surface states with opposite propagation directions on the upper and lower boundaries, respectively [blue and red curves in Fig. 4(a)]. These features are consistent with the effective medium model. We also note that in the effective medium model the upper edge of this nontrivial band gap corresponds to $\mu_{\text{eff}} = 0$, while the lower edge corresponds to $\mu_{\text{eff}} \to \infty$. (See Supplemental Material Sec. I [45].) This feature is consistent with Ref. [47]. However, the interaction in Ref. [47] is short ranged (only limited to particles within a finite distance), but our construction does not make assumptions about the ranges of interactions between particles, and the electromagnetic interaction between particles in the array systems similar to ours is typically not short ranged.

The existence of a one-way edge state in a random system can also be visualized by simulating a finite system as shown in Fig. 4(b). The cylinders are the same as Fig. 4(a) and the minimal distances between cylinders are also kept to be larger than $0.8a$. This lower side of the finite system is truncated by a perfectly matched layer [48] to absorb the wave. The remaining boundaries of the system consist of PEC. The wave propagates anticlockwise without being backscattered when the frequency of the source is inside the nontrivial band gap. While here we show an example of a random lattice, similar effects of the band gap and one-way edge states are also observed in other isotropic systems, such as quasicrystals with the same cylinder and cylinder density. (See Supplemental Material Sec. IV [45].)

In conclusion, we theoretically propose and numerically demonstrate a route towards creating a metamaterial that behaves as a photonic Chern insulator, through homogenization of an array of particles. While for concreteness we have considered cylindrical particles possessing gyromagnetic effects, one can achieve similar results with gyroelectric effects more commonly used in the optical frequency range. Also, the particles can be of other shapes provided that their response can be well described by electric and magnetic polarizabilities. Our method can easily be extended to create metamaterials that achieve electromagnetic analogs of quantum spin Hall systems, and be generalized for other classical wave systems.

This work is supported by the US Air Force of Scientific Research (Grant No. FA9550-12-1-0471), and the US National Science Foundation (Grant No. CBET-1641069). M.X. thanks Dr. S. B. Wang for help with COMSOL simulations.

[1] L. Lu, J. D. Joannopoulos, and M. Soljačić, Nat. Photonics **8**, 821 (2014).

[2] L. Lu, J. D. Joannopoulos, and M. Soljačić, Nat. Phys. **12**, 626 (2016).

[3] S. D. Huber, Nat. Phys. **12**, 621 (2016).
[4] F. D. M. Haldane and S. Raghu, Phys. Rev. Lett. **100**, 013904 (2008).
[5] Z. Wang, Y. D. Chong, J. D. Joannopoulos, and M. Soljačić, Nature (London) **461**, 772 (2009).
[6] Z. Wang, Y. D. Chong, J. D. Joannopoulos, and M. Soljačić, Phys. Rev. Lett. **100**, 013905 (2008).
[7] K. Fang, Z. Yu, and S. Fan, Nat. Photonics **6**, 782 (2012).
[8] Z. Yu, G. Veronis, Z. Wang, and S. Fan, Phys. Rev. Lett. **100**, 023902 (2008).
[9] L. Yuan, Y. Shi, and S. Fan, Opt. Lett. **41**, 741 (2016).
[10] M. C. Rechtsman, J. M. Zeuner, Y. Plotnik, Y. Lumer, D. Podolsky, F. Dreisow, S. Nolte, M. Segev, and A. Szameit, Nature (London) **496**, 196 (2013).
[11] M. Hafezi, E. A. Demler, M. D. Lukin, and J. M. Taylor, Nat. Phys. **7**, 907 (2011).
[12] M. Hafezi, S. Mittal, J. Fan, A. Migdall, and J. M. Taylor, Nat. Photonics **7**, 1001 (2013).
[13] A. B. Khanikaev, S. Hossein Mousavi, W.-K. Tse, M. Kargarian, A. H. MacDonald, and G. Shvets, Nat. Mater. **12**, 233 (2013).
[14] W.-J. Chen, S.-J. Jiang, X.-D. Chen, B. Zhu, L. Zhou, J.-W. Dong, and C. T. Chan, Nat. Commun. **5**, 5782 (2014).
[15] G. Q. Liang and Y. D. Chong, Phys. Rev. Lett. **110**, 203904 (2013).
[16] E. Prodan and C. Prodan, Phys. Rev. Lett. **103**, 248101 (2009).
[17] M. Xiao, G. Ma, Z. Yang, P. Sheng, Z. Q. Zhang, and C. T. Chan, Nat. Phys. **11**, 240 (2015).
[18] Z. Yang, F. Gao, X. Shi, X. Lin, Z. Gao, Y. Chong, and B. Zhang, Phys. Rev. Lett. **114**, 114301 (2015).
[19] C. L. Kane and T. C. Lubensky, Nat. Phys. **10**, 39 (2014).
[20] L.-H. Wu and X. Hu, Phys. Rev. Lett. **114**, 223901 (2015).
[21] R. Süsstrunk and S. D. Huber, Science **349**, 47 (2015).
[22] X. Cheng, C. Jouvaud, X. Ni, S. H. Mousavi, A. Z. Genack, and A. B. Khanikaev, Nat. Mater. **15**, 542 (2016).
[23] F. Gao *et al.*, Nat. Commun. **7**, 11619 (2016).
[24] L. Lu, C. Fang, L. Fu, S. G. Johnson, J. D. Joannopoulos, and M. Soljačić, Nat. Phys. **12**, 337 (2016).
[25] A. Slobozhanyuk, S. H. Mousavi, X. Ni, D. Smirnova, Y. S. Kivshar, and A. B. Khanikaev, Nat. Photonics **11**, 130 (2017).
[26] L. Lu, L. Fu, J. D. Joannopoulos, and M. Soljačić, Nat. Photonics **7**, 294 (2013).
[27] M. S. Rudner, N. H. Lindner, E. Berg, and M. Levin, Phys. Rev. X **3**, 031005 (2013).
[28] M. Xiao, W.-J. Chen, W.-Y. He, and C. T. Chan, Nat. Phys. **11**, 920 (2015).
[29] M. G. Silveirinha, Phys. Rev. B **92**, 125153 (2015).
[30] W. Gao, M. Lawrence, B. Yang, F. Liu, F. Fang, B. Béri, J. Li, and S. Zhang, Phys. Rev. Lett. **114**, 037402 (2015).
[31] F. Liu and J. Li, Phys. Rev. Lett. **114**, 103902 (2015).
[32] M. Xiao, Q. Lin, and S. Fan, Phys. Rev. Lett. **117**, 057401 (2016).
[33] S. A. H. Gangaraj, M. G. Silveirinha, and G. W. Hanson, IEEE J. Multiscale Multiphys. Comput. Technol. **2**, 3 (2017).
[34] M. A. Bandres, M. C. Rechtsman, and M. Segev, Phys. Rev. X **6**, 011016 (2016).
[35] P. Titum, N. H. Lindner, M. C. Rechtsman, and G. Refael, Phys. Rev. Lett. **114**, 056801 (2015).
[36] A. Agarwala, and V. B. Shenoy, Phys. Rev. Lett. **118**, 236402 (2017).
[37] K. A. Arpin *et al.*, Nat. Commun. **4**, 2630 (2013).
[38] S.-H. Kim, S. Y. Lee, S.-M. Yang, and G.-R. Yi, NPG Asia Mater. **3**, 25 (2011).
[39] Y. Xia, B. Gates, and Z. Y. Li, Adv. Mater. **13**, 409 (2001).
[40] J. Zhang, Z. Sun, and B. Yang, Curr. Opin. Colloid Interface Sci. **14**, 103 (2009).
[41] G. W. Milton, D. J. Eyre, and J. V. Mantese, Phys. Rev. Lett. **79**, 3062 (1997).
[42] X. Huang, Y. Lai, Z. H. Hang, H. Zheng, and C. T. Chan, Nat. Mater. **10**, 582 (2011).
[43] F. Liu, Y. Lai, X. Huang, and C. T. Chan, Phys. Rev. B **84**, 224113 (2011).
[44] D. M. Pozar, *Microwave Engineering* (Wiley, Hoboken, NJ, 2012).
[45] See Supplemental Material at http://link.aps.org/supplemental/10.1103/PhysRevB.96.100202 for an effective medium theory for the metamaterials under consideration, band dispersions similar as those in Figs. 1(a)-1(c), projected band structure of the triangular lattice, the evolution of the projected band from a square lattice to random lattices, and one way edge states in the square lattice, the triangular lattice and quasicrystals.
[46] Y. Wu, J. Li, Z.-Q. Zhang, and C. T. Chan, Phys. Rev. B **74**, 085111 (2006).
[47] N. P. Mitchell, L. M. Nash, D. Hexner, A. Turner, and W. T. M. Irvine, arXiv:1612.09267.
[48] J.-P. Berenger, J. Comput. Phys. **114**, 185 (1994).